Applied Catalysis B: Environmental 156–157 (2014) 122–127

Contents lists available at ScienceDirect

Applied Catalysis B: Environmental

journal homepage: www.elsevier.com/locate/apcatb

Photocatalytic hydrogen production over carbon nitride loaded with WS_2 as cocatalyst under visible light

Yidong Hou*, Yongsheng Zhu, Yan Xu, Xinchen Wang

Research Institute of Photocatalysis, State Key Laboratory Photocatalysis on Energy and Environment, Fuzhou University, Fuzhou 350002, China

ARTICLE INFO

Article history:
Received 11 December 2013
Received in revised form 21 February 2014
Accepted 2 March 2014
Available online 12 March 2014

Keywords:
Carbon nitride
WS_2
Cocatalyst
Photocatalytic H_2 evolution

ABSTRACT

Mesoporous graphitic$ carbon nitride (mpg-CN) was loaded with WS_2 via an impregnation–sulfidation approach. The resultant surface heterojunctions between WS_2 and mpg-CN were evidently confirmed with transmission electron microscopy (TEM) and X-ray photoelectron spectroscopy (XPS). Photocatalytic H_2 production on WS_2/mpg-CN under visible light ($\lambda > 420$ nm) shows that WS_2 plays an important role in catalyzing H_2 production. The rate of hydrogen evolution reaches an optimum when the loading amount of WS_2 is about 0.3 at.%. Combined with the physicochemical and electrocatalytic properties of WS_2/mpg-CN, it can be concluded that the enhanced photocatalytic H_2 production activity on WS_2/mpg-CN is mainly attributed to the thin layered junctions formed between WS_2 and mpg-CN and the great performance of WS_2 as a cocatalyst in H_2 evolution reaction.

1. Introduction

Since Fujishima and Honda observed a photoelectrochemical cell using Pt–TiO_2 electrodes for hydrogen evolution under the irradiation of ultraviolet (UV) light in 1972 [1], photocatalytic water splitting for hydrogen production, especially based on earth-abundant semiconductors and co-factors, has drawn considerable attentions as a potential way to solve the energy and environment problems [2–4]. So far, many active photocatalysts, including (oxy)nitrides, (oxy)sulfides, and silicides, for H_2 evolution under visible light have been prepared and reported [5–7]. However, most of these photocatalysts under investigation are expensive, unstable, rare, toxic or difficult to prepare. Thus, it is necessary to develop a new type of photocatalyst with a wide visible-light absorption band, high stability in contact with water, non-toxic, and abundant and so on.

Recently, we found that covalent graphitic carbon nitride (g-CN) solid can work as a new type of visible-light and metal-free photocatalyst with suitable electronic structure (conduction band at −0.8 V and valence band at 1.9 V vs. RHE) covering redox potentials for water splitting [8,9]. However, like many other photocatalysts, g-CN alone shows a very poor electrocatalytic activity for water splitting, and its photocatalytic performance quite relies on surface cocatalysts [10–14]. The cocatalysts interfaced with the light-harvesting semiconductor not only facilitate the charge separation and increase the lifetime of the photo-generated electron/hole pair, but also lower the activation barriers for H_2 or O_2 evolution [15,16]. Thus, the use of cocatalysts can result in an increase in overall photocatalytic performance, including activity, selectivity, and stability. Unfortunately, in most cases, the used cocatalysts are mainly the expensive and scarce platinum group metals or their oxides [17]. Therefore, it is one of the most important tasks to replace noble metal by earth abundant elements toward potential large-scale applications [18]. Among many potential candidates, the cheap transition metal based compounds (such as MoS_2, WS_2, WC, NiS, Co_3O_4) have demonstrated promising activities as the cocatalysts in photocatalytic water splitting reaction [19–23].

In general, the efficiency of a given photocatalytic system is quite dependent on the physical nature of cocatalysts loaded for promoting reductive or/and oxidative catalysis reaction. In particular, the structural characteristics and intrinsic catalytic properties of a cocatalyst are very important [15]. In recent work, we found that MoS_2 is an efficient cocatalyst for the photocatalytic H_2 evolution on mesoporous g-CN (mpg-CN) under visible light as a result of the structural and electronic compatibility between MoS_2 and mpg-CN [13]. Since WS_2 has a similar crystal structure and chemical properties with MoS_2, we expect that WS_2 could be also used as a promoter similar to MoS_2 for mpg-CN in photocatalytic H_2 production.

Herein, we reported that WS_2/mpg-CN junctions were obtained through an impregnation–sulfidation process. The detailed structure and property of the resultant WS_2/mpg-CN were examined.

* Corresponding author. Tel.: +86 591 83773729; fax: +86 591 83779105.
E-mail address: ydhou@fzu.edu.cn (Y. Hou).

http://dx.doi.org/10.1016/j.apcatb.2014.03.002
0926-3373/

It was found that WS_2 demonstrates similar properties to MoS_2 as a cocatalyst, which can also efficiently promote the photocatalytic activity of mpg-CN in H_2 evolution under visible light irradiation.

2. Experiment

2.1. Preparation of catalysts

All the chemicals were reagent grade and used without further purification. mpg-CN was synthesized according to the reported procedure [24]. WS_2/mpg-CN catalysts were prepared via impregnation–sulfidation approach. Certain amounts of tungsten precursor were loaded onto mpg-CN by an impregnation from the solution containing different amounts of $(NH_4)_2WS_4$. After removing water with a rotary evaporator at 50 °C, the $(NH_4)_2WS_4$/mpg-CN precursors were heated at 350 °C for 3 h in flowing 10% H_2S–90% H_2 gas mixture to obtain WS_2/mpg-CN catalysts. The amount of the WS_2 loaded onto mpg-CN was calculated by assuming that the $(NH_4)_2WS_4$ was completely converted to WS_2.

2.2. Characterization of catalysts

Powder X-ray diffraction (XRD) data were collected using a Bruker D8 Advance X-ray diffractometer (Cu K1 irradiation, $\lambda = 1.5406$ Å). Nitrogen adsorption–desorption isotherms were collected at 77 K using Micromeritics ASAP 2020 equipment. Transmission electron microscopy (TEM) measurements were obtained on a FEI Tencai 20 microscope. X-ray photoelectron spectroscopy (XPS) measurements were performed on a Thermo Scientific ESCA Lab250 spectrometer which consists of a monochromatic Al Kα as the X-ray source. All of the binding energies were calibrated by the C1s peak at 284.6 eV. UV–vis diffuse reflectance spectra were collected using a Varian Cary 500 UV–Vis–NIR spectrometer equipped with an integrating sphere, and $BaSO_4$ was as a reference standard. Photoluminescence (PL) spectra were performed on Edinburgh Analytical Instruments FL/FSTCSPC920 coupled with a time-correlated single-photo-counting system. The electrochemical experiments were conducted on a CHI600E workstation.

2.3. Measurement of photocatalytic activity

The photocatalytic reactions were performed in a Pyrex top-irradiation reaction vessel connected to a closed gas circulation and evacuation system. 50 mg of catalyst was suspended in an aqueous solution (100 mL) containing lactic acid (10 vol.%). The reactant solution was degassed several times to remove air prior to irradiation under a Xenon 300 W lamp equipped with various optical cut-off filters to monitor the photocatalytic reaction. The amount of H_2 production was analyzed using an online gas chromatography.

3. Results and discussion

Fig. 1 presents the XRD patterns of as-prepared WS_2/mpg-CN catalysts. It can be seen that mpg-CN has two distinct diffraction peaks at 27.5° and 13.2°, corresponding to the (0 0 2) and (1 0 0) peaks for graphitic materials, respectively. This is in good agreement with the reported [25]. The positions of the diffraction peaks remain almost unchanged for WS_2/mpg-CN catalysts obtained via an impregnation–sulfidation approach. Further observation from Fig. 1 reveals that with the increasing of WS_2 content, the diffraction intensity of mpg-CN slightly decreases after loading with WS_2. However, no characteristic diffraction peaks of WS_2 can be observed. This could be due to the low loading amount and high dispersion of WS_2 in the mpg-CN framework.

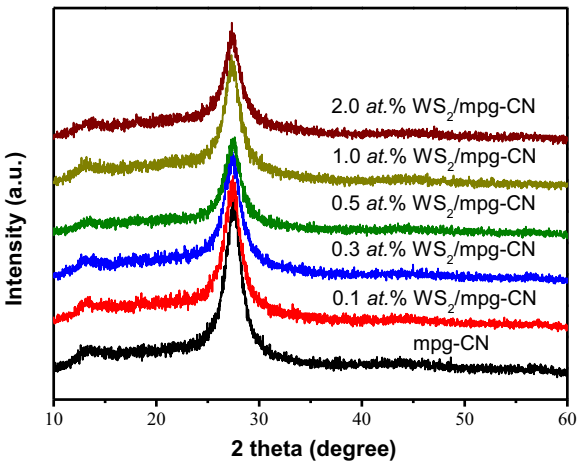

Fig. 1. XRD patterns of mpg-CN and WS_2/mpg-CN.

Nitrogen adsorption–desorption isotherms were used for texture analysis. It can be seen in Fig. 2 that mpg-CN possesses a type H_3 hysteresis loop, implying the presence of mesopores. Textural parameters derived from adsorption–desorption isotherms data are presented in the inserted Table. It can be seen that, comparing with pure mpg-CN, the specific surface area and pore volume of the catalysts decrease largely after loading WS_2. This could be ascribed to the aggregation of nanoparticles and destruction of porous structure of mpg-CN during the impregnation–sulfidation process.

TEM were used to investigate the morphology of WS_2 and the interfacial structure between WS_2 and mpg-CN. As shown in Fig. 3a, WS_2 slabs with characteristic layered structure instead of particles are found on the surface of WS_2/mpg-CN. From HRTEM inserted in Fig. 3a, it is easy to find that the (002) plane of WS_2 grows along the surface of mpg-CN to form intimate junctions between WS_2 and mpg-CN. The chemical composition of WS_2/mpg-CN was then analyzed by using energy-dispersive X-ray spectroscopy (EDX). As displayed in Fig. 3b, the signals assigned to W and S can be easily detected, and which further confirms the existence of WS_2 on the mpg-CN surface. The result of EDX elemental mapping analysis (Fig. S1) verifies that WS_2 is highly dispersed on the surface of mpg-CN. As similar to MoS_2, WS_2 and graphitic carbon nitride have analogous layered structure and the specific property of Van der Waals interaction may provide advantages in the desirable junction formation. Intimate junctions between WS_2 and mpg-CN are indeed formed by via an impregnation–sulfidation approach.

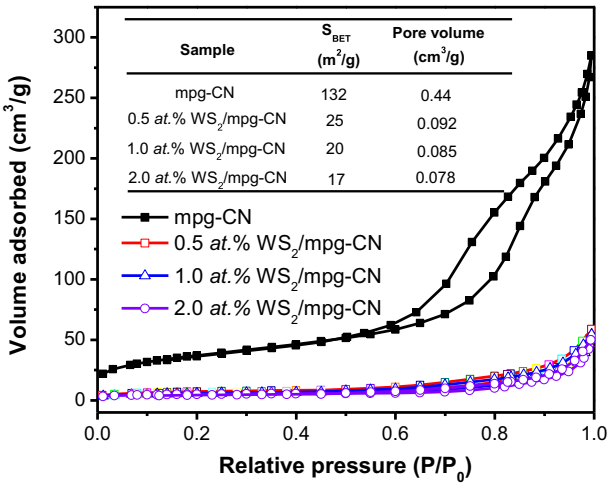

Fig. 2. Nitrogen adsorption–desorption isotherms of mpg-CN and WS_2/mpg-CN.

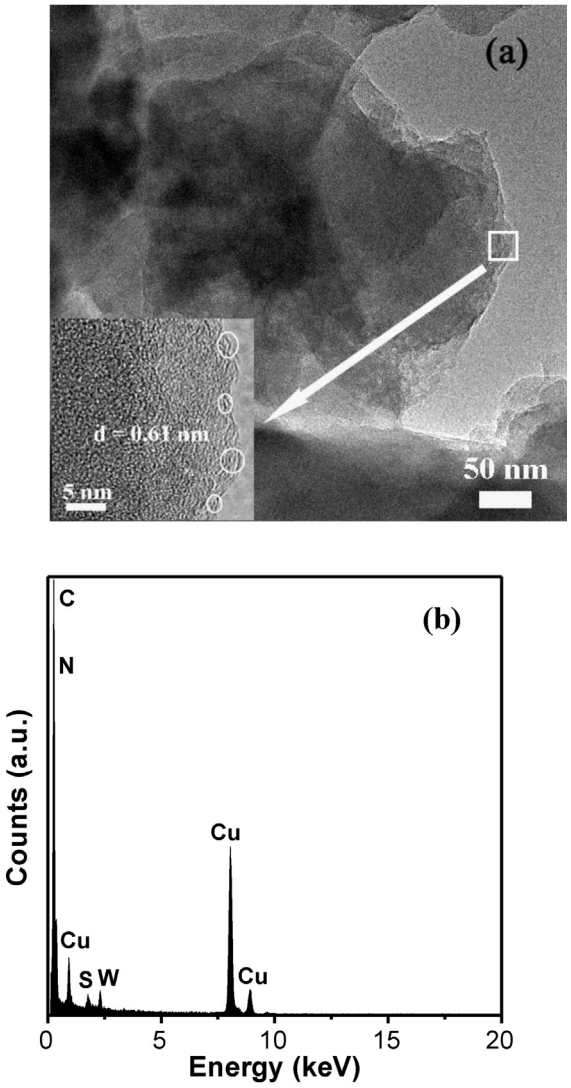

Fig. 3. TEM image (a) and EDX analysis (b) of WS_2/mpg-CN.

Furthermore, the mesoporous structure of mpg-CN facilitates and stabilizes the high dispersion of WS_2 on the mpg-CN surface and the formation of the thin WS_2/mpg-CN intimate junctions [13]. These junctions ensure effective hydrogen evolution by virtue of the light absorption by mpg-CN combined with a short carrier transport distance, and the exposure of a large external surface area for the catalytic reaction. By taking advantage of electron tunneling effect, the thin-layered WS_2 highly dispersed on the mpg-CN surface could also offer much higher efficiency than multi-layered WS_2 for the electron-transporting through the WS_2 layers to reaction interfaces.

The chemical states of WS_2/mpg-CN were investigated by the XPS technique. As displayed in Fig. 4a, O, N, C, S and W elements are observed in the survey spectrum. Fig. 4b presents the W4f core level spectrum with four peaks at 32.1, 34.1, 34.8 and 36.8 eV. The W4f peaks at 32.1 and 34.1 eV can be ascribed to the W^{4+} species, while the other two peaks at higher binding energies can be attributed to W^{6+} species [22]. Combined with the result of S2p core level spectrum (Fig. 4c), it confirms that WS_2 is formed on the surface of mpg-CN. The existence of W^{6+} may be explained by that $(NH_4)_2WS_4$ is not stable during the impregnation process, a considerable amount of $(NH_4)_2WS_4$ suffers from oxidation reaction and results in the formation of tungsten oxide. The binding energy of W shifts to a lower value compared to the reported value [26],

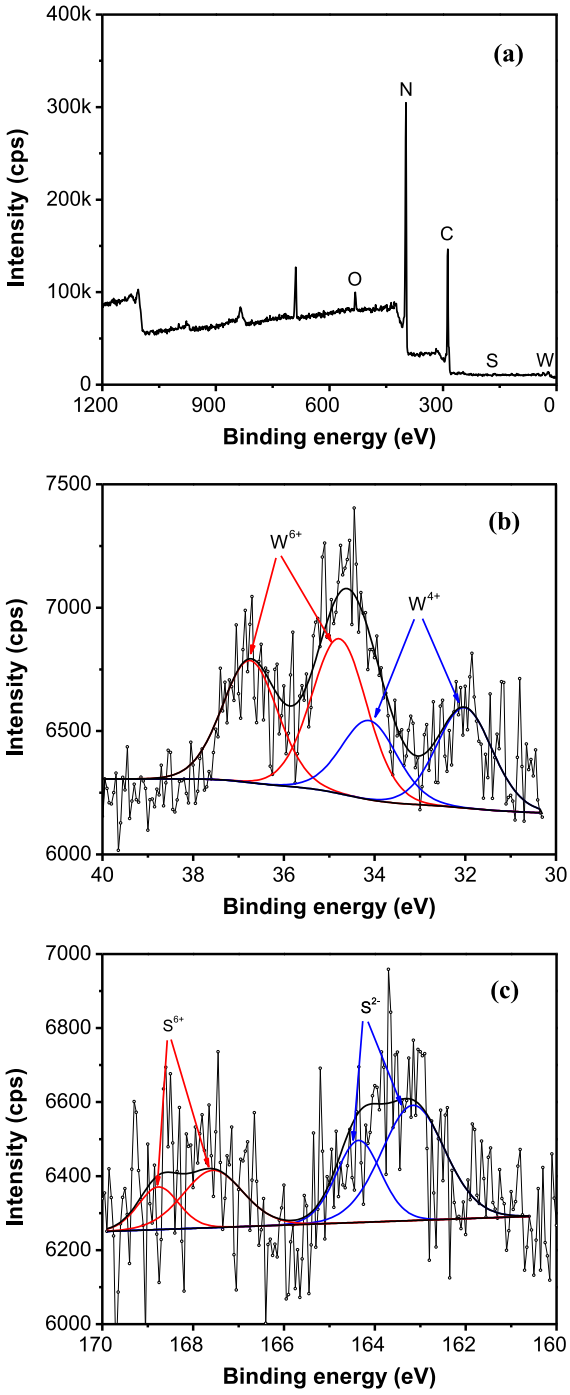

Fig. 4. XPS spectra of WS_2/mpg-CN.

indicative of a strong chemical interaction between the W species and the conjugated mpg-CN [23]. Generally, tungsten oxide gradually transforms to WS_2 with increased sulfidation temperature. Unfortunately, mpg-CN cannot be stabilized at high sulfidation temperature. Thus 350 °C was used as the sulfidation temperature in this study.

Based on the above XPS results analysis, it can be concluded that, WS_2 and WO_3 coexist on the surface of mpg-CN. Since the conduction band of WO_3 situates at a more positive position than the potential of H_2 evolution [27], WO_3 is believed to be inactive for photocatalytic H_2 evolution. Meanwhile, we also annealed the $(NH_4)_2WS_4$/mpg-CN in air to prepare WO_3/mpg-CN, and the

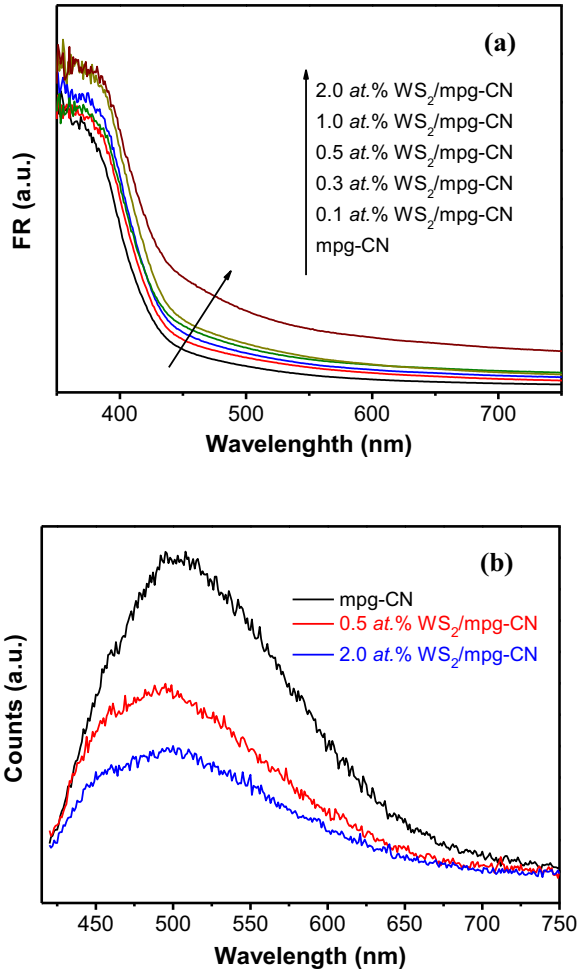

Fig. 5. UV–vis diffuse reflection spectra (a) and photoluminescence spectra (b) of mpg-CN and WS_2/mpg-CN.

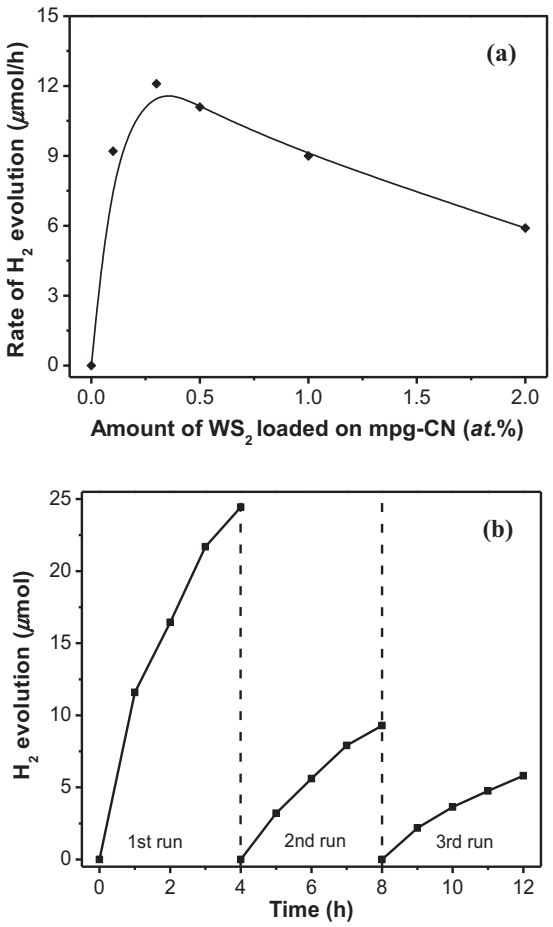

Fig. 6. (a) Rate of H_2 evolution on mpg-CN with loading different amounts of WS_2 under visible light ($\lambda > 420$ nm), (b) cyclic runs for the photocatalytic H_2 production on WS_2/mpg-CN.

obtained WO_3/mpg-CN exhibited negligible activity for photocatalytic hydrogen evolution under visible light. Thus, it is reasonable to consider that the active component for catalytic H_2 evolution is WS_2 rather than WO_3. Therefore, we assume that WS_2 is the only tungsten species loaded onto mpg-CN in the following sections for simplicity.

Fig. 5a displays the UV–vis diffuse reflection spectra of as-prepared WS_2/mpg-CN. The abrupt onset of absorption at ~430 nm is assigned to the electronic transition from the valence band to the conduction band in the graphitic carbon nitride semiconductor upon excitation with light [8]. After loading WS_2, there is a broad absorption shoulder in the spectra. The absorption shoulder corresponds to the optical absorption of WS_2. Fig. 5b gives the photoluminescence spectra of as-prepared catalysts. Obviously, the photoluminescence of mpg-CN is quenched in the presence of WS_2. This occurrence is owing to the efficient charge transfer between WS_2 and mpg-CN, thus leading to an improvement in the separation efficiency of the photo-generated carriers.

No H_2 was detected when WS_2 was supported on inert mesoporous SiO_2 (SBA-15), thus implying that WS_2 alone is not active for photocatalytic H_2 evolution in a wireless system. Pure mpg-CN also showed negligible activity. Fig. 6a shows the rate of H_2 evolution on the WS_2/mpg-CN catalysts. There is a plot of the variation in their activities, showing that the rate of hydrogen evolution increases initially and then reaches an optimum when the amount of the loading of WS_2 is about 0.3 at.%. Further loading of WS_2 on mpg-CN leads to a decrease in the H_2 evolution rate. The decrease in the activity of the catalysts with a heavy loading of WS_2 could be due to the shading effect, which can seriously block the absorption of the incident light by mpg-CN. This hypothesis is strongly supported by the UV–vis diffuse reflection spectra.

We also investigated the rate of photocatalytic hydrogen evolution on WS_2/mpg-CN as a function of cut-off wavelength of the incident light. Fig. S2 reveals that the wavelength dependence of hydrogen evolution rate of WS_2/mpg-CN corresponds well to its optical absorption. This observation supports that the hydrogen evolution process is primarily induced by light-excitation of carbon nitride polymer.

In addition to the photocatalytic activity, the stability of a photocatalyst is also important in practical application. In order to study the stability of WS_2/mpg-CN, the cycling hydrogen evolution experiments were performed. As shown in Fig. 6b, the rate of H_2 evolution on WS_2/mpg-CN decreased with every reaction cycle. To reveal the reason for the deactivation during activity test, we did the comparisons of XRD and XPS analysis on the fresh and used WS_2/mpg-CN. The XRD analysis result shows that the crystal structure of WS_2/mpg-CN does not change after the photocatalytic test (Fig. S3). The fresh and used photocatalyst give similar N1s and C1s core level spectra shown in Fig. S4, this further confirms the high stability of mpg-CN. However, significant changes are observed in W4f and S2s core level spectra (Fig. S4). The data (Table 1) obtained after deconvolution of these peaks reveal that the atomic ratio of W^{6+}/N increases and that of S^{2-}/N decreases for the catalyst after test. This means that the oxidation/corrosion of WS_2 by the

Table 1
Values of W and S species to N in the fresh and used WS_2/mpg-CN.

Sample	W/N (at.%)			S/N(at.%)		
	W^{4+}	W^{6+}	W (sum)	S^{2-}	S^{6+}	S (sum)
WS_2/mpg-CN (fresh)	0.13	0.21	0.34	0.68	0.25	0.93
WS_2/mpg-CN (used)	0	0.25	0.25	0	0	0

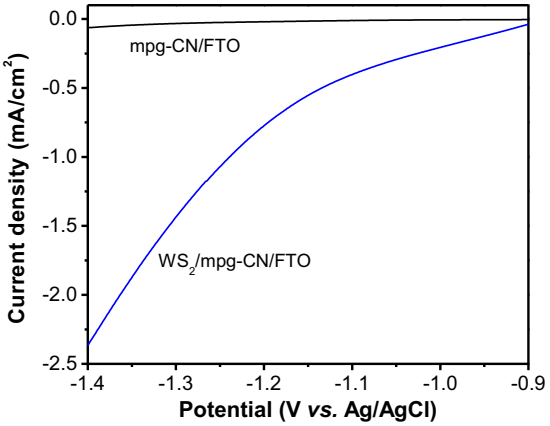

Fig. 7. Polarization curves of mpg-CN/FTO and WS_2/mpg-CN/FTO electrodes.

photo-generated holes occurs on WS_2/mpg-CN catalyst, accounting for the deactivation during the cycling runs. Of course, more work is required to improve the activity and particularly stability of WS_2/mpg-CN for potential application, for example to release charge built-up by using oxidative cofactors to promote the transfer of the holes from the bulk to the surface.

It is well regarded that the reduction of protons to H_2 is a very important step in the photocatalytic H_2 production reaction. It has been reported that, the catalytic characteristics of MoS_2 for H_2 evolution is a very important factor for the enhanced activity in photocatalytic water splitting system [13,28]. In this study, electrochemical measurements were conducted to investigate the role of WS_2. Fig. 7 shows the polarization curve of the WS_2/mpg-CN/FTO electrode together with that of mpg-CN/FTO as a control. Cathodic current observed in the potential range from −0.9 to −1.4 V vs. Ag/AgCl corresponds to the reduction of water to H_2. In comparison with mpg-CN/FTO electrode, WS_2/mpg-CN/FTO electrode shows much enhanced cathodic current. Apparently, WS_2 is a good catalyst that can efficiently catalyze the H_2 evolution, thus enhances the rate of H_2 evolution on WS_2/mpg-CN. Moreover, because of the anisotropic conductivity of WS_2, like MoS_2 [29], thin-layered WS_2 can lessen the poor charge transport from layer to layer and shorten the electron transport time and distance, thus improves the efficiency in the utilization of photo-generated electrons for hydrogen production.

On the basis of the above results, the mechanism for the photocatalytic H_2 production on WS_2/mpg-CN is proposed. As shown in Scheme 1, upon photo-excitation, electrons and holes are generated in the conduction band (CB) and valence band (VB) of mpg-CN, respectively. The photo-generated carriers move toward the catalyst surface, the holes oxidize the lactic acid and the electrons reduce protons to H_2. However, because mpg-CN itself is not active for H_2 evolution, the photo-generated electrons and holes are likely to recombine, resulting in the low photocatalytic activity. The presence of WS_2 facilitates the transfer of the photo-generated electrons from mpg-CN to WS_2, and protons can be efficiently reduced to produce H_2 because WS_2 can serve as an active site for hydrogen evolution. Moreover, the formed thin-layered junctions promote the electron transfer from mpg-CN to WS_2. These cofactors are supposed to be the main reasons why the WS_2/mpg-CN exhibited enhanced activity of hydrogen evolution.

4. Conclusion

The H_2 production performance of mpg-CN under visible light is significantly improved by loading WS_2. The rate of hydrogen evolution reaches an optimum when the amount of WS_2 loaded is about 0.3 at.%. Similar to MoS_2, the geometric similarity in the layered

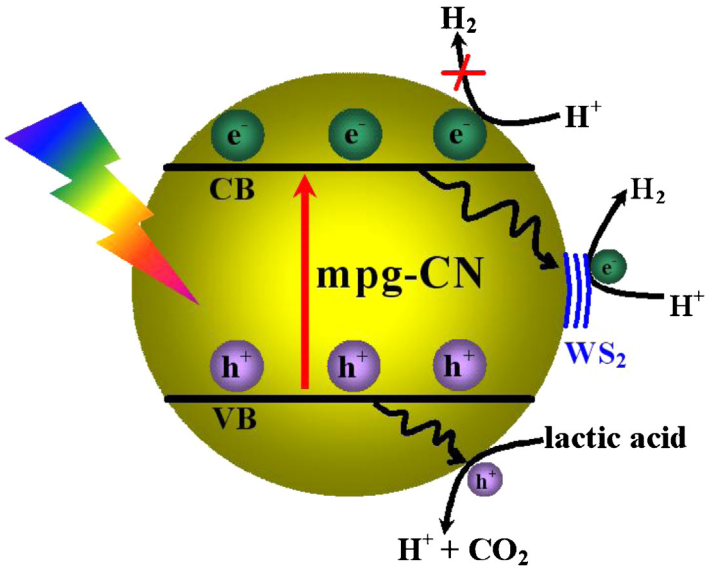

Scheme 1. Proposed reaction mechanism for photocatalytic H_2 evolution on WS_2/mpg-CN.

structure of WS_2 and mpg-CN and the mesoporous structure of mpg-CN facilitate the planar growth of WS_2 on the mpg-CN surface and the formation of the thin planar WS_2/mpg-CN interface. These characteristics are supposed to be mainly responsible for the enhanced photocatalytic activity of WS_2/mpg-CN catalysts. This work demonstrates a possibility for the use of WS_2 as a substitute for noble metals as cocatalyst in the photocatalytic H_2 production. It also provides useful information in design and fabricating effective interfacial junctions between cocatalysts and semiconductors.

Acknowledgements

The work was supported by 973 Program (2013CB632405), NSFC (21203030 and 21033003), Specialized Research Fund for the Doctoral Program of Higher Education Program (20113514120001) and Program for New Century Excellent Talents in University of Fujian Province (JA13020).

Appendix A. Supplementary data

Supplementary data associated with this article can be found, in the online version, at http://dx.doi.org/10.1016/j.apcatb.2014.03.002.

References

[1] A. Fujishima, K. Honda, Nature 238 (1972) 37–38.
[2] J.A. Turner, Science 305 (2004) 972–974.
[3] N.S. Lewis, D.G. Nocera, Proc. Natl. Acad. Sci. U. S. A. 103 (2006) 15729–15735.
[4] M. Pelaez, N.T. Nolan, S.C. Pillai, M.K. Seery, P. Falaras, et al., Appl. Catal. B Environ. 125 (2012) 331–349.
[5] A. Kudo, Int. J. Hydrogen Energy 31 (2006) 197–202.
[6] F.E. Osterloh, Chem. Mater. 20 (2008) 35–54.
[7] X.B. Chen, S.H. Shen, L.J. Guo, S.S. Mao, Chem. Rev. 110 (2010) 6503–6570.
[8] X.C. Wang, K. Maeda, A. Thomas, K. Takanabe, G. Xin, et al., Nat. Mater. 8 (2009) 76–80.
[9] J.S. Zhang, X.F. Chen, K. Takanabe, K. Maeda, K. Domen, et al., Angew. Chem. Int. Ed. 49 (2010) 441–444.
[10] K. Maeda, X.C. Wang, Y. Nishihara, D.L. Lu, M. Antonietti, et al., J. Phys. Chem. C 113 (2009) 4940–4947.
[11] Y. Di, X.C. Wang, A. Thomas, M. Antonietti, ChemCatChem 2 (2010) 834–838.
[12] A.T. Garcia-Esparza, D. Cha, Y. Ou, J. Kubota, K. Domen, et al., ChemSusChem 6 (2013) 168–181.
[13] Y.D. Hou, A.B. Laursen, J.S. Zhang, G.G. Zhang, Y.S. Zhu, et al., Angew. Chem. Int. Ed. 52 (2013) 3621–3625.
[14] L. Ge, C.C. Han, X.L. Xiao, L.L. Guo, Appl. Catal. B Environ. 142–143 (2013) 414–422.
[15] K. Maeda, K. Domen, J. Phys. Chem. Lett. 1 (2010) 2655–2661.
[16] J.H. Yang, D.G. Wang, H.X. Han, C. Li, Acc. Chem. Res. 46 (2013) 1900–1909.
[17] M.G. Walter, E.L. Warren, J.R. Mc-Kone, S.W. Boettcher, Q.X. Mi, et al., Chem. Rev. 110 (2010) 6446–6473.
[18] P.C.K. Vesborg, T.F. Jaramillo, RSC Adv. 2 (2012) 7933–7947.
[19] X. Zong, H.J. Yan, G.P. Wu, G.J. Ma, F.Y. Wen, et al., J. Am. Chem. Soc. 130 (2008) 7176–7177.
[20] J.S. Jang, D.J. Ham, N. Lakshminarasimhan, W. Choi, J.S. Lee, Appl. Catal. A Gen. 346 (2008) 149–154.
[21] W. Zhang, Y. Wang, Z. Wang, Z. Zhong, R. Xu, Chem. Commun. (2010) 7631–7633.
[22] X. Zong, J.F. Han, G.J. Ma, H.J. Yan, G.P. Wu, et al., J. Phys. Chem. C 115 (2011) 12202–12208.
[23] J.S. Zhang, M. Grzelczak, Y.D. Hou, K. Maeda, K. Domen, et al., Chem. Sci. 3 (2012) 443–446.
[24] X.C. Wang, K. Maeda, X.F. Chen, K. Takanabe, K. Domen, et al., J. Am. Chem. Soc. 131 (2009) 1680–1681.
[25] A. Thomas, A. Fischer, F. Goettmann, M. Antonietti, J. Muller, et al., J. Mater. Chem. 18 (2008) 4893–4908.
[26] A. Di-Paola, L. Palmisano, A.M. Venezia, V. Augugliaro, J. Phys. Chem. B 103 (1999) 8236–8244.
[27] Y. Xu, M.A.A. Schoonen, Am. Miner. 85 (2000) 514–523.
[28] X. Zong, G.P. Wu, H.J. Yan, G.J. Ma, J.Y. Shi, et al., J. Phys. Chem. C 114 (2010) 1963–1968.
[29] H. Tributsch, J.C. Bennett, J. Electroanal. Chem. 81 (1977) 97–111.